Supporting Information

How Does a Plasmon-Induced Hot Charge Carrier Break a C–C Bond?

Hyun Huh, Hoa Duc Trinh, Dokyung Lee, and Sangwoon Yoon*

Department of Chemistry, Chung-Ang University, 84 Heukseok-ro, Dongjak-gu, Seoul 06974, Korea.

*E-mail: sangwoon@cau.ac.kr

1. SERS Spectra of MBA in NPoM when Irradiated at 785 nm (Enlarged Spectra)

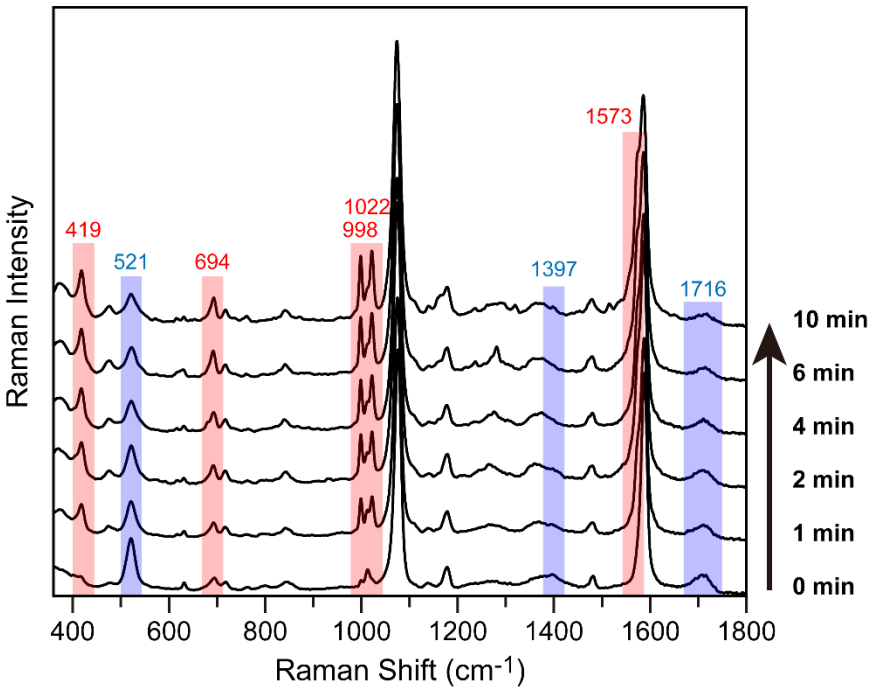

Figure S1. Time evolution of the SERS spectrum of MBA in NPoM nanogaps upon irradiation at 785 nm; the irradiation time periods are given on the right. For clarity, each spectrum is an enlargement of that depicted in Figure 2. The peaks shaded in the red increase in intensity, whereas those shaded in the blue decrease as the reaction proceeds.

2. SERS Spectra of Possible Products

We find that new peaks appear in the SERS spectrum of MBA NPoM upon irradiation at 785 nm. To identify the origins of these new peaks, we acquired SERS spectra of a few possible products, including BT, BTP, and MP (Figure S2). The comparison unambiguously shows that irradiation at 785 nm converts the MBA molecules in the nanogaps into BT.

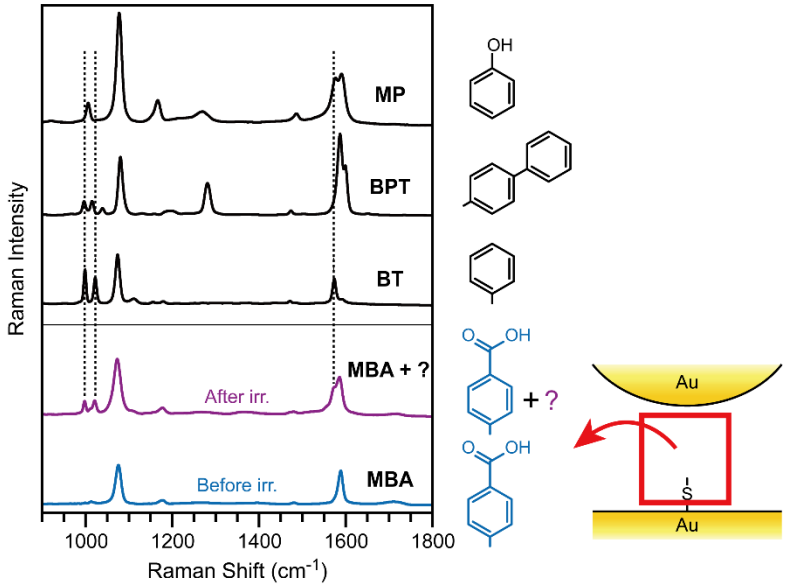

Figure S2. SERS spectra of MBA in nanogaps before and after irradiation at 785 nm (lower panel). SERS spectra of BT, BPT, and MP in similar nanogap systems (upper panel). By comparing these spectra, the new peaks that appear in the spectrum of MBA following irradiation are found to correspond to BT.

3. Power Dependence

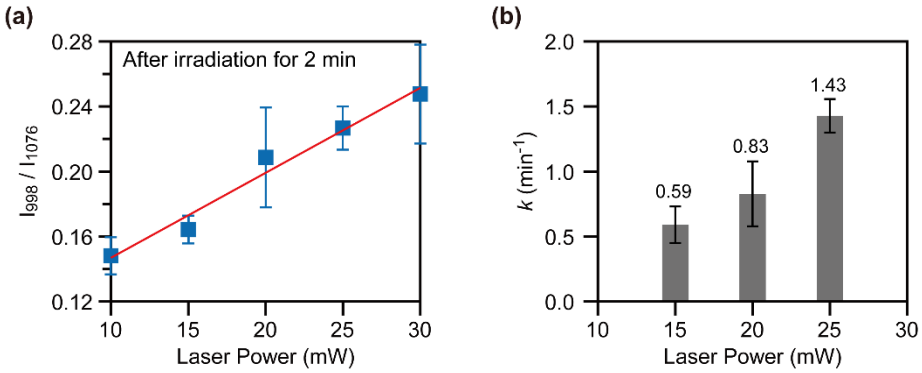

Figure S3. (a) Changes in the reaction yield (represented by the intensity of the product peak at 998 cm^{-1}) with the reaction laser power ranging from 10 to 30 mW. The peak intensities were measured after irradiation of the sample for 2 min. The yield increases linearly with power. (b) The reaction rate constant obtained by exponential fitting (as in Figure 2b) at each designated reaction laser power.

4. Excitation of the Au@SiO_2 NPoM at Different Wavelengths for the Plasmon-Driven Decarboxylation of MBA in Nanogaps

Irradiation at 785 nm drives the decarboxylation reaction of MBA in the nanogaps between the AuNPs and Au substrates (Figure 2). Wavelength-dependent experiments clearly show that resonant excitation of surface plasmons is required to drive the reaction (Figure 3). Hot charge carriers (electrons and holes) produced by the decay of the excited surface plasmons are presumably transferred to the carboxylate anions, which leads to decarboxylation. Our observation that the simple replacement of AuNPs with silica-coated AuNPs (Au@SiO_2) in the same NPoM structures does not yield the reaction product strongly supports the hot charge-carrier transfer mechanism (Figure 4). Silica shells block hot charge-carrier transfer from AuNPs to the surface molecules (in this case, carboxylate anions), as reported previously;[1] consequently the decarboxylation reaction does not proceed. However, it is also possible that irradiation at 785 nm fails to excite the surface plasmons of the Au@SiO_2 NPoM system, in contrast to the Au NPoM system. The gap between the AuNPs and the Au substrate is larger for the former than the latter because of the presence of the 2.8-nm thick silica shell. According to the plasmon hybridization model, the larger gap (hence, weaker coupling) is likely to reduce the shift to lower energy of the dipole plasmon mode.[2] Hence, the resonance plasmon energy of Au@SiO_2 NPoM corresponds to a shorter wavelength than that of Au NPoM, and excitation at 785 nm no longer resonates with the plasmon energy of the Au@SiO_2 NPoM.

We explored this possibility using plasmon excitations of different wavelength. Figure S4 shows that MBA does not decarboxylate, even when the Au@SiO_2 NPoM system is excited at wavelengths shorter than 785 nm (*i.e.*, 633 and 532 nm). We do not observe the characteristic BT product peaks at 998 and 1022 cm^{-1} in any of the excitation experiments at 532, 633, or 785 nm. This result strongly suggests that the lack of decarboxylation in the Au@SiO_2 NPoM system is not associated with unexcited surface plasmons from off-resonance conditions, but rather to the blocked transfer of hot charge carriers that are generated by excited surface plasmons.

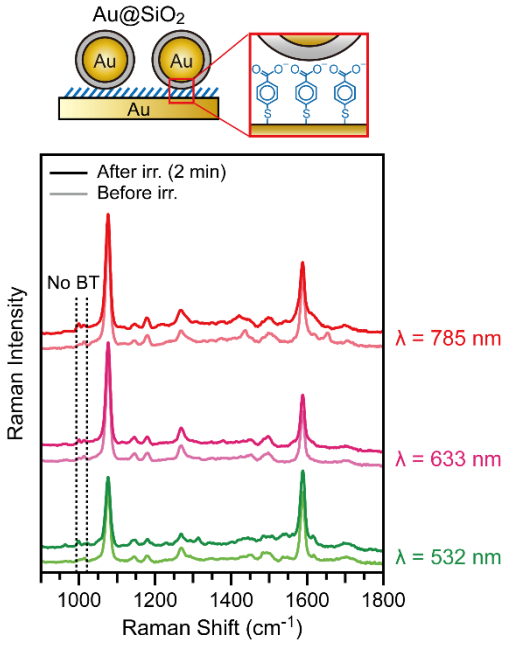

Figure S4. SERS spectra of MBA in the Au@SiO_2 NPoM system before (faint spectrum) and after (bold spectrum) irradiation at 785, 633, and 532 nm. No BT peaks (998 and 1022 cm^{-1}, positions indicated by dotted lines) are observed in these three cases. The irradiation power is 15 mW at all three wavelengths. The SERS spectra are obtained at 785 nm, with a power of 6.0 mW, and 3 s total exposure time. The spectra are offset for clarity.

We also considered the following factors that may influence the reaction in using the silica shell to discriminate between the hot-carrier-transfer reaction and the thermal reaction.

(1) Porous structure of the silica shell

It is well known that the silica shell has a porous structure. Small molecules in solution often penetrate through the shell into the surface of the AuNP at the core. However, we dropcast the Au@SiO_2 particles onto the *dry* MBA SAMs. Thus, it is not likely that MBA molecules desorb from the Au substrate overcoming the van der Waals forces in the SAM and diffuse all the way into the core AuNP. Thus, porosity of the silica shell does not influence the reaction.

(2) Tunneling

Hot charge carriers can still tunnel through the silica shell. Tunneling may occur not because of the shell thickness (2.8 nm), but because of the pinholes in the shell. The tunneling probability changes with the potential energy barrier height and width. The 2.8-nm insulating gap seems far enough to ignore the tunneling effect. However, if there are many pinholes inside the shell, the effective

distance that the charge carriers must tunnel through is reduced and the charge-carrier transfer to the outside of the shell may be possible. The fact that we did not observe the decarboxylation reaction from the Au@SiO_2 NPoM indicates that tunneling is not significant and the silica shell works well as an insulating gap.

(3) Binding of the carboxylic acid to the surface of silica shell

The carboxylic acid (or carboxylate) group of MBA may bind to the silanol (OH–Si) or siloxide (O^-–Si) of the surfaces of the silica shell, which may hinder the decarboxylation reaction. However, we did not observe any peak shifts in the Raman spectra of MBA in the Au@SiO_2 NPoM, compared to the bare Au NPoM, that are attributable to the formation of new bond between the carboxylic acid (or carboxylate) and the surface of the silica shell. Higher resolution measurements and more rigorous spectral analysis will reveal whether this chemical bonding is feasible.

5. Mechanism for Plasmon-Driven β-Cleavage Reaction of 4-Mercaptobenzyl Alcohol (MBnOH)

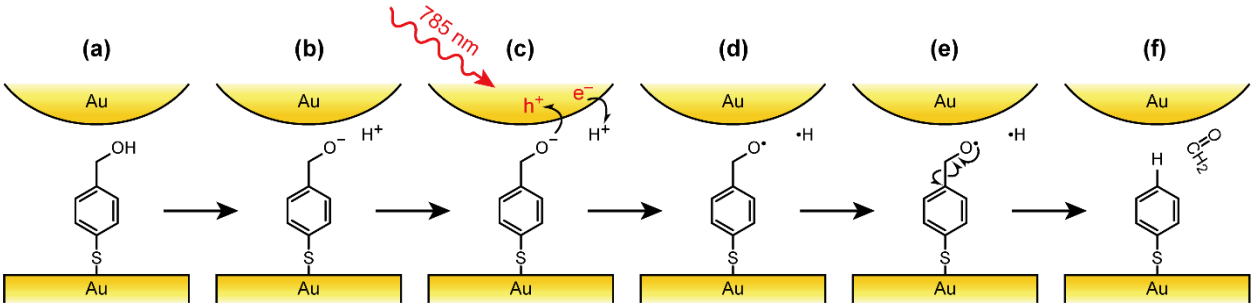

Figure S5. The proposed mechanism for the decarboxylation reaction (Figure 8) can be applied to other bond cleavage reactions. Shown here is the β-cleavage reaction of MBnOH in nanogaps (a). Similarly to the decarboxylation of MBA, MBnOH must be deprotonated to form hydroxide anions first (b). Hot holes and electrons generated by resonant excitation of surface plasmons transfer to hydroxide anions and protons, respectively (c), which produces hydroxyl radicals and hydrogen atoms (d). Subsequently, the hydroxyl radical undergoes the β-cleavage reaction, leading to the formation of the BT radical and formaldehyde (e). Finally, the BT radical reacts with hydrogen atoms to form the BT product (f).

6. Experimental Methods

6.1 Materials

The following materials are used as received. From Sigma Aldrich: gold(III) chloride trihydrate (≥99.9%), sodium citrate dihydrate (≥99.0%), (3-aminopropyl)trimethoxysilane (APTMS, 97%), sodium silicate solution (SiO_2~26.5%), 4-mercaptobenzoic acid (MBA, 99%), benzenethiol (BT, 97%), 4-methylbenzenethiol (MBT, 98%), 4-mercaptophenol (MP, 97%), sodium hydroxide (NaOH, >97.5%), and biphenyl-4-thiol (BPT, >96.5%). From other suppliers: methyl 4-mercaptobenzoate (MBA-Me, >98%, Santa Cruz Biotechnology), 4-mercaptobenzyl alcohol (MBnOH, ≥90%, Santa Cruz Biotechnology), hydrochloric acid (HCl, 35.0–37.0%, Duksan Chemical), sulfuric acid (H_2SO_4, >95%, Duksan Chemical), hydrogen peroxide (H_2O_2, >34.5%, Daejung Chemical), argon gas (99.999%, Air Korea), bare AuNPs (70 nm, Nanopartz), and water (HPLC grade, J. T. Baker).

6.2 Synthesis of Au Nanoparticles (AuNPs)

We use the seeded growth method reported by Puntes and coworkers.[3] To produce AuNP seeds, $HAuCl_4$ solution (0.5 mL, 25.5 mM) is injected into a boiling solution of sodium citrate (78 mL, 2.3 mM). The color of the solution changes from yellow to dark gray, and then to red over 10 min. The solution is cooled to 90 °C, after which the amounts of the chemicals listed in Table S1 are added sequentially from stock solutions of $HAuCl_4$ (25.5 mM) and sodium citrate (60.5 mM), and allowed to react for the times indicated. The temperature is maintained at 90 °C during the reaction, and the solution is vigorously stirred. The AuNP solutions (15 mL) are centrifuged at 4500 rpm for 30 min and redispersed in water (15 mL) to remove residual species prior to any experiment.

Table S1. Growth step reaction conditions

Step	Added reagent	Added volume (mL)	Reaction time (min)
Seed		78.5	
1^{st} growth	$HAuCl_4$	0.5	30
	$HAuCl_4$	0.5	30
2^{nd} growth	H_2O	75	until temp = 90°C
	Citrate	3	5
	$HAuCl_4$	1.5	30
	$HAuCl_4$	1.5	30

3rd growth	H_2O	150	until temp = 90°C
	Citrate	3	5
	$HAuCl_4$	1.5	30
	$HAuCl_4$	1.5	30
4th growth	H_2O	184	until temp = 90°C
	$HAuCl_4$	1.5	30
	$HAuCl_4$	0	30

We determine the sizes of the AuNPs by transmission electron microscopy (TEM). The AuNPs prepared as described above have an average diameter of 61.3 ± 8.2 nm (*N* = 331). The localized surface plasmon resonance (LSPR) band of the AuNPs is observed at 538 nm (Figure S6).

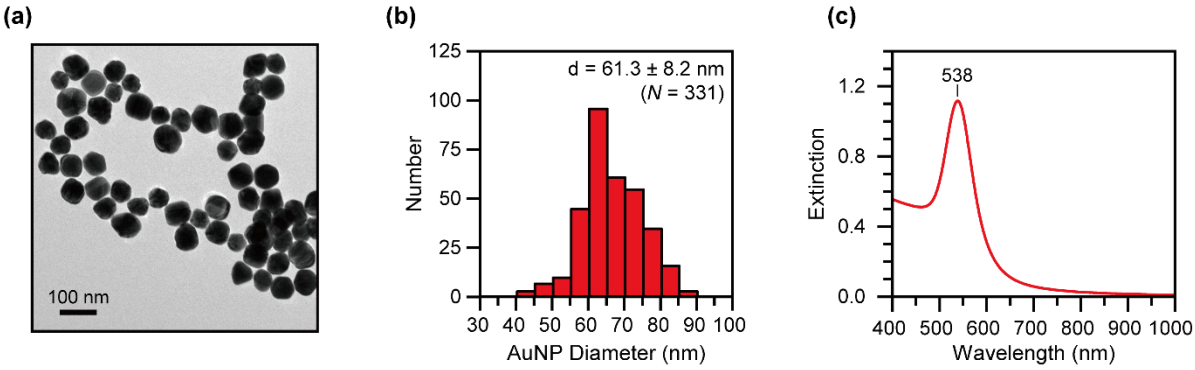

Figure S6. (a) A representative TEM image, (b) size distribution, and (c) UV-vis spectrum of the synthesized AuNPs.

6.3 Synthesis of Silica-Coated Au Nanoparticles (Au@SiO_2)

We follow the method reported by Tian and coworkers for preparing the silica-coated AuNPs (Au@SiO_2).[4] We add an aqueous solution of APTMS (0.4 mL, 1 mM) to a AuNP solution (30 mL, 49 pM) with vigorous stirring. After 15 min, sodium silicate solution (3.2 mL, 0.54% SiO_2, adjusted to pH 10 with HCl) is added and the solution is stirred for 3 min at room temperature. The solution is then transferred to a hot water bath at 90 °C and stirred for 2 h. The solution is finally centrifuged twice at 4500 rpm for 30 min and the Au@SiO_2 particles are collected.

6.4 Construction of NPoM

NPoM is constructed by adsorbing AuNPs onto the surfaces of MBA SAMs on Au substrates. The Au substrates (150-nm thick Au films deposited on Ti-coated (10-nm thick, 4" Si wafers) are purchased from

the National Nanofab Center (NNFC, Daejeon, Korea). The Au substrates are cut into 1 cm × 1 cm pieces and cleaned with piranha solution (H_2SO_4:H_2O_2 = 7:3) for 10 min to remove organic impurities. After washing with water and drying with N_2 gas, the Au substrates are immersed in thiol solution (2 mL, 1 mM) for 16 h in the dark, which leads to the formation of thermodynamically stable and highly ordered thiol-molecule SAMs on the Au substrates. The SAM/Au substrates are washed with ethanol for 3 min and dried with N_2. To create nanogaps, we take 3 μL of the AuNP solution and place a droplet onto a SAM/Au substrate. Drying under low vacuum (V4880-071, Simatech Industrial Co.) for 0.5–1 h completes the formation of NPoM system.

Notably, the dropcast AuNPs form a coffee ring pattern as the solvent evaporates, which carries the AuNPs outwards.[5] Hence, the AuNPs are distributed sparsely near the center and are more densely distributed toward the outside of the ring. The AuNPs aggregate along the arc of the circle. Because we want to explore nanogaps between the AuNPs and the Au substrate, rather than gaps between AuNPs, we perform experiments in the region between the center and the periphery of the circle where the AuNPs are well dispersed. Figure S7 shows representative scanning electron microscopy (SEM) images of the NPoM region used. AuNPs are adsorbed on the MBA SAMs and are relatively well dispersed. We find that, on average, 150 AuNPs are located inside the focal area (diameter: 5 μm) of the laser when using a 50× objective.

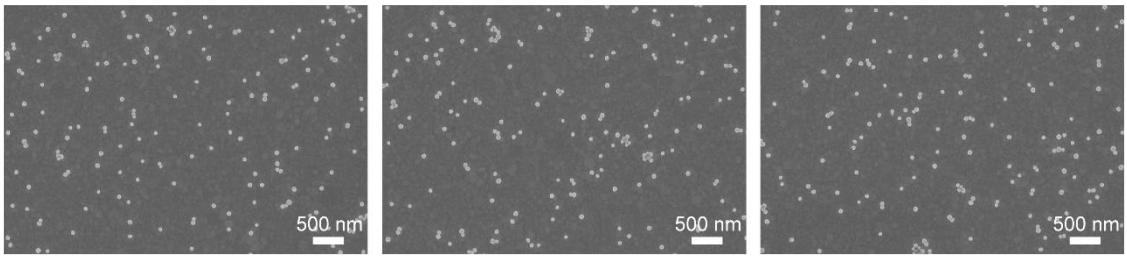

Figure S7. Representative SEM images acquired from NPoM regions (AuNPs on MBA SAMs) in which the experiments are performed.

6.5 pH Adjustment

To change the protonation state of the carboxyl group of MBA, we adjust the NPoM pH (Figure 5 in the main text). We first prepare HCl (0.1 M) and NaOH (0.225 M) solutions and dilute these solutions to pH 3 and 11.5, respectively. Deionized water is used as the neutral medium. The pH is measured with a pH meter (Mettler-Toledo) after calibration with three standard buffer solutions (pH 4.01, 7.00, and 9.21). To

adjust the NPoM pH, we drop an aliquot of the required prepared solution onto the NPoM and allow them to react for 10 min, after which the sample is dried.

6.6 Ambient-Gas Exchange

Experiments are usually performed with samples exposed to air. We use a homebuilt gas-flow cell to adjust the ambient-gas conditions (Figure S8). The cell is a small chamber with a quartz window and inlet and outlet tubes. The inlet tube is connected to an Ar gas cylinder *via* a flow controller (RMA-12-SSV, Dwyer). The outlet tube is immersed in silicone vacuum oil to prevent backflow. To introduce water vapor into the chamber, we insert a water bubbler in the Ar gas line. The gas flows in at a rate of 300 cm^3/min in these experiments. The cell is purged for at least for 30 min in order to ensure that the internal air is completely replenished with the desired gas.

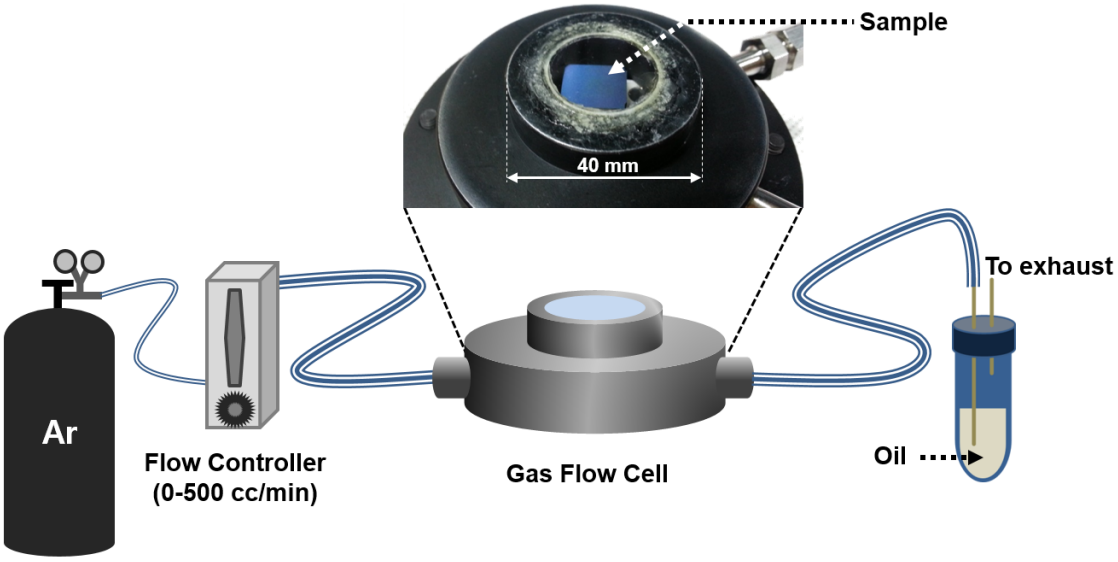

Figure S8. A schematic illustration and a photography of our homebuilt gas-flow cell.

6.7 Laser Irradiation and Raman Spectroscopy

The prepared NPoM is placed under a microscope objective for laser-induced reactions and Raman spectroscopy. Three lasers, with wavelengths of 785 nm (Invictus, Kaiser Optical Systems), 633 nm (633-MLD, Cobolt), and 532 nm (Excelsior 532, Spectra Physics) are used in these reactions. The 532- and 633-nm laser beams are introduced to the microscope (Leica DMLP) through the back port of an illuminator. The diffuser and the lenses inside the illuminator are removed in order to maintain collimated laser beams. The laser light is reflected off a dichroic mirror (705 DRLP, Omega Optics) and focused onto the sample

though objective lenses. The 785-nm laser beam is delivered from the top by an optical fiber and directly focused onto the sample through objectives. The laser power is measured at the sample using a 10× objective (Leica NPLAN, 10×, N.A. 0.25, w.d. 17.6 mm) because the working distance (w.d.) of the 50× objective (Leica NPLAN, 50×, N.A. 0.75, w.d. 0.5 mm) is too small to accommodate the power meter probe head (PD300-UV, Ophir). The laser spot size after the 10× objective is 26 μm. We typically use a laser power of 15 mW, which corresponds to 2800 W/cm^2.

For plasmon-driven reaction experiments, the laser is focused on the sample through the 50× objective. The product is detected by Raman spectroscopy. For Raman experiments, the 785-nm laser (6.0 mW) is focused on the reaction region through the 50× objective; Raman scattering is collected by the same objective and transmitted to the spectrometer (Raman Rxn 1, Kaiser Optical Systems) equipped with a holographic transmissive grating and a CCD detector. The total exposure time for a typical experiment is 3 s. When the gas flow cell is mounted on the stage, a 10× objective (w.d. 17.6 mm) is used for both reaction and Raman spectroscopy in order to properly focus the lasers on the sample, which are positioned further away from the objective due to the cell dimensions; accordingly, the reaction-laser power is raised to 50 mW to compensate for the lower photon density. A low (6.0 mW) SERS-laser power is maintained.

References

(1) Takeyasu, N.; Yamaguchi, K.; Kagawa, R.; Kaneta, T.; Benz, F.; Fujii, M.; Baumberg, J. J. Blocking Hot Electron Emission by SiO_2 Coating Plasmonic Nanostructures. *J. Phys. Chem. C* **2017**, *121*, 18795-18799.

(2) Nordlander, P.; Oubre, C.; Prodan, E.; Li, K.; Stockman, M. I. Plasmon Hybridization in Nanoparticle Dimers. *Nano Lett.* **2004**, *4*, 899-903.

(3) Bastús, N. G.; Comenge, J.; Puntes, V. Kinetically Controlled Seeded Growth Synthesis of Citrate-Stabilized Gold Nanoparticles of up to 200 nm: Size Focusing *versus* Ostwald Ripening. *Langmuir* **2011**, *27*, 11098-11105.

(4) Li, J.-F.; Li, S.-B.; Anema, J. R.; Yang, Z.-L.; Huang, Y.-F.; Ding, Y.; Wu, Y.-F.; Zhou, X.-S.; Wu, D.-Y.; Ren, B.; Wang, Z.-L.; Tian, Z.-Q. Synthesis and Characterization of Gold Nanoparticles Coated with Ultrathin and Chemically Inert Dielectric Shells for SHINERS Applications. *Appl. Spectrosc.* **2011**, *65*, 620-626.

(5) Chang, W.-S.; Slaughter, L. S.; Khanal, B. P.; Manna, P.; Zubarev, E. R.; Link, S. One-Dimensional Coupling of Gold Nanoparticle Plasmons in Self-Assembled Ring Superstructures. *Nano Lett.* **2009**, *9*, 1152-1157.